

NON-LOCAL ALPHA ENERGY DEPOSITION EFFECTS  
IN TORSATRON REACTORS

Joseph W. Johnson  
Lawrence M. Lidsky

PFC/RR-82-11

April 9, 1982

## Non-Local Alpha Energy Deposition Effects in Torsatron Reactors

### *Abstract*

The behavior of the temperature profiles in torsatrons is compared for the cases of local and non-local alpha energy deposition. A numerical model of the plasma is developed, in which the flux surfaces remain stationary. The non-local energy deposition results in slightly higher temperatures (6 per cent on axis) required for ignition and a 15 per cent lower temperature growth rate. These non-local effects are larger at lower densities. Both cases are found to be stable against step perturbations in the electron temperature.

Financial support for this project was provided by a fellowship from the General Electric Foundation.

## Contents

|  |    |
|--|----|
| <b>Table of Contents</b> . . . . .                               | 3  |
| <b>List of Figures</b> . . . . .                                 | 4  |
| <b>List of Tables</b> . . . . .                                  | 4  |
| <b>Section 1 Introduction</b> . . . . .                          | 5  |
| <b>Section 2 The Energy Balance Equations</b> . . . . .          | 5  |
| 1. Diffusion Coefficients . . . . .                              | 5  |
| 2. Radiation Losses and Energy Transfer . . . . .                | 6  |
| 3. Alpha Particle Heating . . . . .                              | 7  |
| 4. Density Related Terms . . . . .                               | 9  |
| <b>Section 3 Particle Density Equations</b> . . . . .            | 11 |
| <b>Section 4 Ignition Requirements</b> . . . . .                 | 12 |
| <b>Section 5 Time Evolution of the Temperature</b> . . . . .     | 18 |
| <b>Section 6 Stability of the Steady State Regimes</b> . . . . . | 24 |

Section 7 Summary and Conclusions . . . . . 24

References . . . . . 26

### List of Figures

Fig. 1 Local case,  $T_o = 6.8$  keV . . . . . 15

Fig. 2 Local case,  $T_o = 6.9$  keV . . . . . 15

Fig. 3 Non-Local case,  $T_o = 7.2$  keV . . . . . 16

Fig. 4 Non-Local case,  $T_o = 7.3$  keV . . . . . 16

Fig. 5 Local case,  $T_o = 8.0$  keV . . . . . 21

Fig. 6 Non-Local case,  $T_o = 8.0$  keV . . . . . 21

Fig. 7 Local case,  $R_o = 24$  m,  $T_o = 8$  keV . . . . . 23

Fig. 8 Non-Local case,  $R_o = 24$  m,  $T_o = 8$  keV . . . . . 23

### List of Tables

Table 1 Non-Local Energy Deposition Matrix . . . . . 10

Table 2 Local Energy Deposition Matrix . . . . . 10

Table 3 Non-Local Energy Deposition Matrix,  $R_o = 24$  m . . . . . 17

Table 4 Local Energy Deposition Matrix,  $R_o = 24$  m . . . . . 17

Table 5 Local Equilibrium Conditions . . . . . 22

Table 6 Non-Local Equilibrium Conditions . . . . . 22

## Section 1. Introduction

The torsatron magnetic confinement device is of considerable interest for controlled fusion applications. In this paper, the time dependent behavior of the electron and ion temperature profiles in a typical torsatron reactor is studied. Recently, the non-local nature of the alpha heating source has been quantified<sup>[1]</sup>, i.e. the amount of energy deposited in each region due to alpha particles born in any region of the plasma has been calculated. The goal of this work is to determine the effect of this non-local energy deposition on the ignition characteristics and stability of the plasma.

Three issues of interest will be examined here: first, the different ignition requirements for the local and non-local cases; second, the difference in the time evolution of the temperature profiles; and third, the stability of the local and non-local equilibria will be studied.

The  $l = 3$  torsatron plasma studied here has the physical parameters of the A-machine described in reference 1: major radius= 48 m, winding minor radius= 4 m, toroidal flux at the separatrix= 82.8 Wb, average minor radius of the separatrix= 2.1 m, and the magnetic field on the axis= 5.5 T.

## Section 2. The Energy Balance Equations

The energy balance equations are obtained by taking velocity moments of the Vlasov equation. The result is<sup>[2,3]</sup>:

$$\frac{3}{2}n \frac{\partial T}{\partial t} = Q + \nabla \cdot k \nabla T \quad (1)$$

where  $k$  is the thermal conductivity and  $Q$  is the net heat source. The assumption is made in the derivation is that  $\underline{u}$ , the average species velocity, is zero. Also, the magnetic flux surfaces are assumed to remain fixed in space.

Equation 1 can be reduced to one-dimensional form by flux surface averaging<sup>[4,5]</sup>. The approximation that no temperature or density gradients can exist along field lines is made. Because the field lines lie on surfaces of constant flux, both the temperature and the density will depend only on the flux. The flux surface averaged equation is<sup>[3]</sup>:

$$\frac{3}{2}n \frac{\partial T}{\partial t} = \frac{\partial \psi}{\partial V} \frac{\partial}{\partial \psi} \left( k (\nabla \psi)^2 \frac{\partial V}{\partial \psi} \frac{\partial T}{\partial \psi} \right) + Q \quad (2)$$

where  $V$  is the volume enclosed by the flux surface.

### 2.1. Diffusion Coefficients

The ion thermal conductivity in torsatrons is predicted to exhibit a plateau-like behavior<sup>[1]</sup> over a wide range of collision frequencies. This is very similar to the neoclassical theory for axisymmetric

systems. The calculations of reference 1 were done at an ion temperature of 8 keV; to use these results for the ion and electron thermal conductivities, the scaling of the diffusion coefficient with temperature and particle mass must be determined.

The neoclassical ion diffusion coefficient in the perpendicular direction is given by<sup>[6]</sup>:

$$\chi_{\perp i} = \frac{3\sqrt{\pi}\epsilon^2 r_{ci} c T_i}{2|\Theta|r e H_o} \quad (3)$$

where  $\epsilon = a/R$  is the aspect ratio,  $H_o$  is the toroidal magnetic field,  $\Theta = ir/2\pi R$ ,  $i$  is the rotational transform, and  $r_{ci} = v_{ti}/\omega_{ci} = c\sqrt{2T_i m_i}/eB$  is the ion Larmor radius. The only temperature dependent factors are  $T_i$  and  $r_{ci}$ . Together they give  $\chi_{\perp i} \approx T_i^{3/2}$ . From reference 1, we know that  $\chi_{\perp i}(8\text{keV}) = D_{plat}$ , the plateau level. Thus we can write

$$\chi_{\perp i}(T_i) = D_{plat} \left( \frac{T_i}{8} \right)^{3/2} \quad (4)$$

For the electrons, an equation similar to equation (3) can be written. The temperature scaling remains the same, and the only mass dependent quantity is the Larmor radius. Thus the electron diffusion coefficient is smaller than the ion diffusion coefficient by a factor of the square root of the mass ratio.

$$\chi_{\perp e} = D_{plat} \sqrt{\frac{m_e}{m_i}} \left( \frac{T_e}{8} \right)^{3/2} \quad (5)$$

There is some experimental evidence which shows that the electron diffusion coefficient may be larger than that given by this neoclassical scaling.

To obtain the thermal conductivities from the diffusion coefficients, equations (4) and (5) must be multiplied by the ion and electron densities, respectively. Because the thermal conductivity depends on  $\psi$  through the temperature and the density, it must remain inside the  $\psi$  derivative in equation (2).

## 2.2. Radiation Losses and Energy Transfer

Two radiation processes are included in the energy balances; these are bremsstrahlung and cyclotron radiation. Line radiation has been neglected because impurity effects are not included in this model. At the temperatures which will be of interest in this work, recombination radiation is negligible compared to bremsstrahlung<sup>[8]</sup>. Also, ion cyclotron radiation will be neglected in comparison with electron cyclotron radiation.

The energy lost per unit volume by the electrons due to Bremsstrahlung can be expressed in terms of the species densities and the electron temperature<sup>[7,8]</sup>.

$$W_{brem} = 4.85 \times 10^{-37} T_e^{1/2} Z_{eff} n_e^2 \quad (6)$$

where  $T_e$  is in keV,  $n_e$  is in  $m^{-3}$  and  $n_e Z_{eff} = n_i + 4n_\alpha$ .

The energy loss due to electron cyclotron radiation can be expressed<sup>[5,9]</sup> in terms of the magnetic field and the electron temperature and density.

$$W_{cyc} = 2.02 \times 10^{-10} B^{2.5} n_e^{1/2} T_e^2 R_0^{-1/2} \quad (7)$$

where  $B$  is the magnetic field in tesla and  $R_0$  is the major radius in meters.

The electron and ion temperatures are coupled through two terms. The first is the alpha heating term, which will be discussed in the next subsection. The second is the direct collisional transfer of energy. The energy transferred can be written as<sup>[5,8]</sup>:

$$W_{ei} = 2.4 \times 10^{-35} n_z n_e \log \Lambda \frac{(T_e - T_i)}{T_e^{3/2}} \quad (8)$$

where

$$\log \Lambda = \log \left( \frac{4.897 \times 10^{17} T_e^{3/2}}{Z_{eff} \sqrt{n_e}} \right)$$

is the Coulomb logarithm, and

$$n_z = \sum_{species} \frac{nZ^2}{A} = \frac{n_i}{2 + \epsilon} + n_\alpha$$

with  $A$  being the mass number and  $\epsilon$  is the tritium ratio. (It should be noted that the alpha particles are assumed to be in thermal equilibrium with the ions after they have lost their initial 3.5 MeV.)

### 2.3. Alpha Particle Heating

In the torsatron plasma considered here, the only source of energy is the thermalization of the alpha particles born in the fusion reaction. External heating has not been considered. It will be assumed that the alpha particles are thermalized instantaneously. In this discussion of alpha heating, there are three important elements: the reaction rate, the partitioning of the energy between the electrons and ions, and the spatial distribution of the alpha energy.

The alpha energy source term is just the product of the reaction rate density and the energy of a single alpha particle:

$$W_\alpha = 5.6 \times 10^{-13} n_i^2 \epsilon (1 - \epsilon) \langle \sigma v \rangle \quad (9)$$

where  $\epsilon$  is the tritium ratio. (Note: all of the energy terms are in units of Watts/meter<sup>3</sup> throughout this paper).  $W_\alpha$  depends on the ion temperature through  $\langle \sigma v \rangle$ , which has a broad peak at approximately 70 keV. A numerical expression for  $\langle \sigma v \rangle$  is given in reference 5.

$$\langle \sigma v \rangle = \frac{3.68 \times 10^{-18} \exp(-19.94/T_i^{0.33})}{T_i^{0.66} (1 + T_i/70)^{1.33}} \quad (10)$$

Equation (10) is a numerical fit to experimental data. It differs from the data by 10 to 30 per cent, which is comparable to the experimental error in the cross section measurements.

To quantify the partition of energy between the ions and electrons, two parameters are defined;  $f_e$  is the fraction of energy which goes to the electrons, and  $f_i$  is the fraction which goes to the ions.  $f_e$  and  $f_i$  are defined such that  $f_e + f_i = 1$ . The fraction of energy which escapes from the plasma will be considered as part of the spatial factor.

A relation for  $f_e$  is given in reference 10. The expression given is not a simple algebraic formula so the following equation<sup>[5]</sup> is used instead.

$$f_e = 2x \left( \frac{1}{2x} - \frac{1}{6} \log \left( \frac{1 - \frac{1}{\sqrt{x}} + \frac{1}{x}}{(1 + \frac{1}{\sqrt{x}})^2} \right) - \frac{1}{\sqrt{3}} \tan^{-1} \left( \frac{\frac{2}{\sqrt{x}} - 1}{\sqrt{3}} \right) - \frac{1}{\sqrt{3}} \tan^{-1} \left( \frac{1}{\sqrt{3}} \right) \right) \quad (11)$$

where  $x = 0.0093T_e$ . This expression gives values for  $f_e$  within 2.5 per cent of those given in reference 10, for  $T_e < 40$  keV. At higher temperatures, equation (11) will underestimate the energy given to the electrons by as much as 25 percent.

Equations (10) and (11) make it apparent that the alpha heating term in both the electron and ion energy equations is a function of the electron and ion temperatures.

The object of this work is to determine the effect of the non-local alpha energy deposition. To model the spatial effects, a matrix is used to quantitatively define the relationship between the region where the alpha particle is born and the regions where it deposits its energy. To calculate the matrix, alpha particle orbits are simulated by numerically integrating the particle guiding center equations (see reference 1). The particles are followed from birth until thermalization for the confined particles, or until the particle escapes from the plasma. For a confined, well circulating particle, this means following the



particle for  $\approx 5000$  poloidal orbits<sup>[1]</sup>. A four dimensional phase space grid (three flux coordinates and the cosine of the pitch angle) was used to keep track of the phase space regions in which the particle lost energy as it slowed down. For each initial location in phase space, many particles were followed and their energy deposition profiles were averaged. For our purposes, two of the flux coordinates and the pitch angle are integrated out, and the energy deposition profile gives the relationship between the initial  $\psi$  grid location and the amount of energy deposited at each  $\psi$  grid point.

The calculation was done for a grid with 4096 locations per reactor module. There were 4 steps in the toroidal direction, 8 steps in the poloidal direction, 16 steps in the cosine of the pitch angle and 8 steps in the flux direction. By considering alpha particles starting at each of the 8  $\psi$  locations, the energy deposition profiles give the eight by eight matrix shown in Table 1. Reading along the *i*th row gives the fraction of the alpha energy produced in region *i* which is deposited in each region. The sum of the entries in any row is always less than 1. This is because some of the alpha energy escapes from the plasma, due mostly to the birth of alpha particles on unconfined orbits<sup>[1]</sup>.

Table 2 contains the matrix used in the local energy deposition case. This matrix was derived from the non-local matrix by adding the coefficients along each row, to get the alpha "non-escape" probability for each region. The non-escape probability was then placed on the diagonal of an otherwise zero matrix. The result is that the alpha particle either is lost, or it deposits its energy in the region in which it first appeared. By deriving the local matrix in this manner, the percentage of alpha energy confined is the same for both cases; the only difference is in the spatial distribution of the energy.

#### 2.4. Density Related Terms

For each region there will be three additional terms in the energy balances. The first is the energy lost or gained because the particles supplied in the refueling process have a different temperature than the local species temperature. The second is the loss of energy due to particles diffusing out of a region. The third is the gain in energy due to particles diffusing into a region.



### Section 3. The Particle Density Equations

In this work, there are four species which must be accounted for: electrons, deuterons, tritons and alpha particles. The alpha particles are assumed to deposit their energy in the various regions instantaneously. Thus we will be concerned only with the thermal alpha particle diffusion. The problem is simplified by defining the ion density to be the sum of the deuteron and triton densities. To retain information about all four species, the tritium ratio  $\epsilon$  is defined as the ratio of the tritium density to the ion density. In this paper  $\epsilon$  will always be  $= 1/2$ .

As shown in section 3.1, the electron thermal diffusion coefficient is much smaller than the ion thermal diffusion coefficient. The same is true of the particle diffusion coefficients, which are related to the thermal diffusion coefficients. It will be assumed that the electron particle diffusion is negligible, and the electron density may be found from the quasi-neutrality condition.

$$n_e = n_i + 2n_\alpha \quad (12)$$

The equation which describes the evolution of the density profile of a given species is:

$$\frac{\partial n}{\partial t} + \nabla \cdot \Gamma = S \quad (13)$$

which is just the continuity equation with  $\Gamma = n\mathbf{u}$  and a source term  $S$ .  $\Gamma$ , the particle flux, can be expressed in terms of the density gradient using Fick's Law. In flux surface coordinates this becomes:

$$\Gamma = -D(\nabla\psi) \frac{\partial n}{\partial\psi} \quad (14)$$

where  $D$  is the particle diffusion coefficient.

The particle diffusion coefficient is related to the thermal diffusion coefficient. As electron particle diffusion has been neglected, expressions for only the ion and alpha particle diffusion coefficients are needed. Experimentally, it has been found that the particle confinement time is larger than the energy confinement time by a factor of between 3 and 8. This implies that the particle diffusion coefficient is smaller than the thermal coefficient by the same factor. It turns out that the particle diffusion effects in the regime of interest are insensitive to the value of this constant. Thus the ion particle diffusion coefficient can be expressed using equation (4).

$$D_i = \frac{1}{3}\chi_{\perp i} = \frac{1}{3}D_{plat} \left( \frac{T_i}{8} \right)^{\frac{3}{2}} \quad (15)$$

The thermal alpha diffusion coefficient is related to the ion coefficient by the mass ratio.

$$D_\alpha = \sqrt{\frac{m_\alpha}{m_i}} D_i \quad (16)$$

where  $T_\alpha = T_i$  has been assumed.

The net source term for the ions is simply the difference between the loss of ions in the fusion reaction and ions added by refueling. The alpha source term is the number of alpha particles created. It will be assumed that the number of thermalized alpha particles deposited in one region can be determined by the same matrix which describes the energy deposition. Thus the fraction of particles deposited in region  $j$  which were born in region  $i$  is the same as the fraction of energy due to particles born in region  $i$  which is deposited in region  $j$ .

#### Section 4. Ignition Requirements

In this section, the initial values of the temperatures needed to insure ignition of the plasma are compared for the local and non-local cases. In this discussion, a plasma is ignited when the energy density increases over a finite period of time. A difference between the local and non-local cases is expected on the basis of Tables 1 and 2. In the non-local case, the inner regions produce more energy (sum along the rows) than they receive (sum along the columns). Intuitively, one expects that higher initial temperatures will be needed for this case; the greater reaction rate will offset the non-local losses in the inner regions.

The computer code TORSE<sup>[3]</sup> was run for different initial values of the temperatures until the point at which the plasma is ignited is found. The initial conditions are of the form<sup>[1]</sup>:

$$n = n_o \left( 1 - \frac{\psi}{\psi_{sep}} \right)^{P_n} \quad \text{and} \quad T = T_o \left( 1 - \frac{\psi}{\psi_{sep}} \right)^{P_T} \quad (17)$$

where  $T_o, n_o$  are the values on the axis; and  $P_n$ , and  $P_T$  are parameters which determine how peaked the profiles are. The values used here are<sup>[1]</sup>:  $P_n = 0.13$  and  $P_T = 0.39$ . The same values of  $T_o, n_o, P_n$  and  $P_T$  are used for the electron and ion initial conditions.

The procedure used was to vary  $T_o$  in equation (17). The density profiles and the peaking parameters of the profiles were left unchanged. The "default refueling" mode of TORSE was used; the ions are replaced as fast as they are lost. The refueling temperature was set to zero, to simulate cold refueling.

For the local case, ignition was obtained at  $T_o = 6.9$  keV. For each value of  $T_o$  that was tried, two plots were generated: the integrated neutron power vs. time and the maximum ion temperature vs. time (the electron temperature shows the same behavior as the ion temperature and will not be considered here). Figure 1(a,b) contains these plots for  $T_o = 6.8$  keV. The neutron power,  $W_n$ , dies away rapidly, but the ion temperature shows an initial rise. This is because the regions near the axis are heating up, but the bulk of the plasma is not ignited. Finally, the thermal diffusion between regions causes the maximum temperature to fall (the horizontal line in the temperature plot indicates that the maximum temperature is at the separatrix—this is held constant as one of the boundary conditions). Figure 2(a,b) shows the same quantities as in Figure 1, except that the initial conditions were generated with  $T_o = 6.9$  keV. The growth of the neutron power and the temperature indicates that the plasma is ignited.

For the non-local case, the centerline temperature had to be raised to 7.3 keV before the plasma was ignited. Figure 3(a,b) was generated with  $T_o = 7.2$  keV and for Figure 4(a,b)  $T_o = 7.3$  keV. In Figure 3, the plasma is not ignited, the behavior of the temperature is as described in the local case at 6.8 keV. When the temperature is raised, it is apparent that the plasma is ignited with  $T_o = 7.3$  keV. As expected, the non-local energy deposition is not favorable from the standpoint of ignition. The plasma temperature has to be raised by approximately 0.4 keV to overcome the non-local effect.

So far we have considered only a relatively high centerline density of  $3 \times 10^{20} \text{ m}^{-3}$ . The ignition requirements for two other densities were also investigated. With the density on axis set to  $1 \times 10^{20} \text{ m}^{-3}$ , neither the non-local nor the local energy deposition case was ignited. This is for centerline temperatures between 6 and 32 keV. With the density increased to  $2 \times 10^{20}$ , the local case is ignited at 9.4 keV. The centerline temperature was varied between 6 and 32 keV but the non-local case did not ignite. Thus, the non-local alpha energy deposition has a greater impact on the ignition requirements at lower densities.

The ignition requirements are also affected by the relative magnitude of the diagonal and non-diagonal terms in the energy deposition matrix. As a limiting case, a uniform energy deposition matrix was used. In this matrix, each coefficient was set to 0.11. This case was studied, using  $n_o = 3.0 \times 10^{20}$ , and with the centerline temperature as high as 30 keV, and it was found that the plasma did not ignite.

Further studies of the ignition requirements were made with the matrices in Tables 3 and 4. These are the non-local and local matrices calculated in reference 1 for a torsatron with a major radius of 24 m, as compared with the  $R_o = 48$  m torsatron we have considered so far. Comparing the local matrices in

Tables 2 and 4, it is apparent that the alpha particles are not as well confined in the smaller torsatron. A comparison of Tables 1 and 3 shows that the non-local nature of the energy deposition matrix is more pronounced in the smaller machine, i.e. the relative magnitudes of the diagonal coefficients are less for the  $R_0 = 24$  case.

Using a centerline density of  $3 \times 10^{20}$ , the centerline temperature is varied to find the minimum temperature at which the plasma is ignited. In the local case, the plasma is ignited at 7.3 keV. This is 0.4 keV higher than the previous local ignition temperature. The increase is due to the poorer alpha confinement, which reduces the heat source. The non-local case is ignited at  $T_0 = 8.0$  keV, which is 0.7 keV higher than the local case. In the  $R_0 = 48$  case, this difference was only 0.4 keV.

(Note: in using the matrices calculated for the  $R_0 = 24$  case, the change in the diffusion coefficient  $D_{plat}$  was neglected, so that the only difference between the two cases was in the alpha heating term. From reference 1,  $D_{plat}$  for the smaller machine is approximately twice the value in the  $R_0 = 48$  machine. With the higher value of  $D_{plat}$ , it is found that the smaller torsatron is not ignited for temperatures on axis of between 8 and 32 keV.)

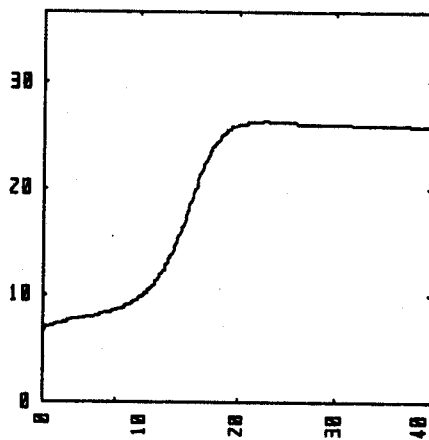
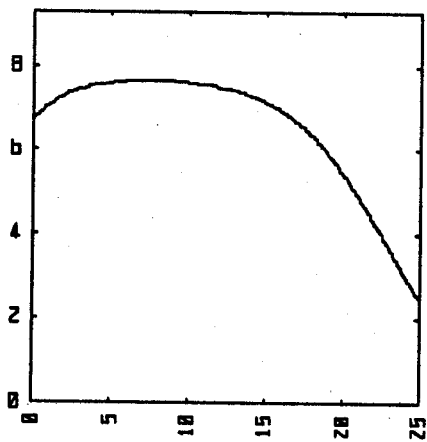
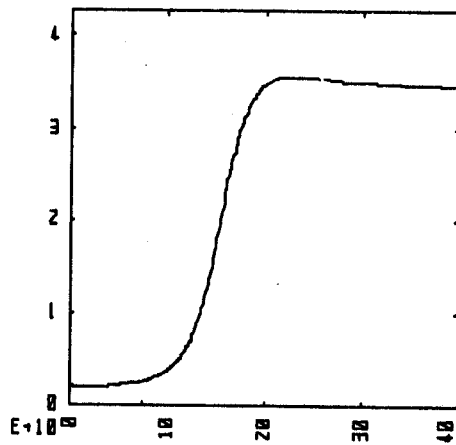
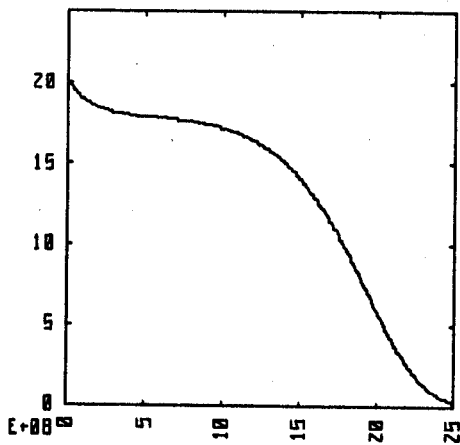


Figure 1: Local case  $T_0 = 6.8$  keV

Figure 1(a):  $W_n$  vs. time

Figure 1(b):  $T_i$  vs. time

Figure 2: Local case  $T_0 = 6.9$  keV

Figure 2(a):  $W_n$  vs. time

Figure 2(b):  $T_i$  vs. time

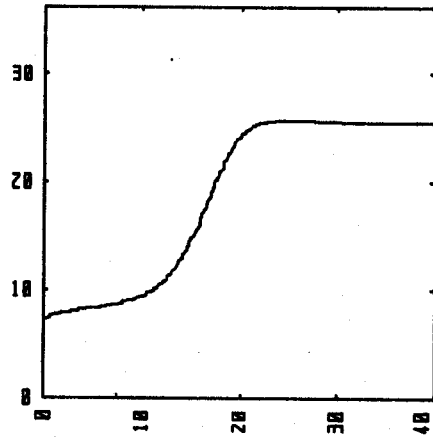
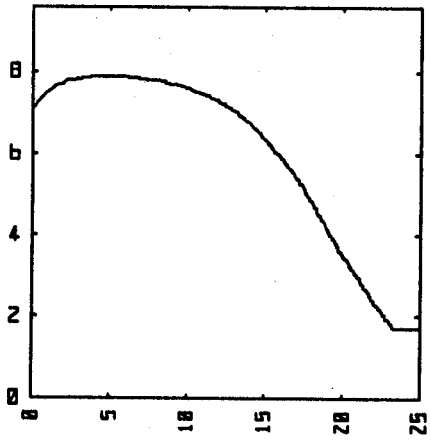
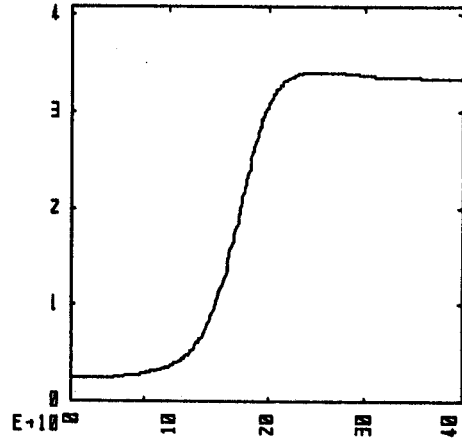
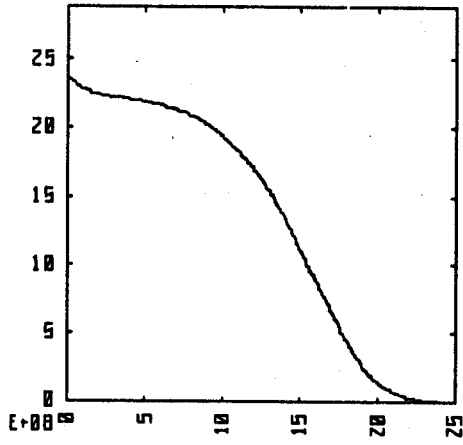


Figure 3: Non-Local case  $T_o = 7.2$  keV

Figure 3(a):  $W_n$  vs. time

Figure 3(b):  $T_i$  vs. time

Figure 4: Non-Local case  $T_o = 7.3$  keV

Figure 4(a):  $W_n$  vs. time

Figure 4(b):  $T_i$  vs. time





## Section 5. Time Evolution of the Temperature

In this section, the time behavior of the temperature and density profiles for the local and non-local cases is examined. We consider here a plasma with a centerline temperature of 8 keV and a centerline density of  $3.0 \times 10^{20} \text{ m}^{-3}$ . With these initial conditions, the plasma will be ignited for both cases. The default refueling mode of TORSE is used. The effect of using this refueling mode is to keep the energy loss associated with refueling small by adding only as many particles as are lost, while keeping the reaction rate from decreasing. This effectively prevents the density from decreasing at every mesh point. In the outer regions of the plasma, the density will actually increase, because the increase in temperature of the inner regions will increase the particle diffusion rate near the center, which leads to accumulation near the edge. As before, the refueling temperature is set to zero.

The computer code is run until a steady state regime is reached. Because the equilibria are calculated by following the time evolution of the energy and density equations for over 100 seconds of model time (steady state is reached after approximately 30 seconds), the equilibria will be stable. Stability against finite perturbations in the electron temperature will be examined in the next section.

Figure 5(a,b,c) consists of three plots, the integrated neutron power, maximum electron temperature, and the maximum ion temperature, as functions of time, for the local case. The steady state conditions are given in Table 5 (The very large thermal output in both Tables 5 and 6 is due to the relatively high temperatures and densities, it is more useful to think of this quantity as being related to the reaction rate averaged temperature). All three graphs show similar behavior; a period of slow growth, followed by a rapid increase to a maximum, and a gradual decrease to the steady state. The transition from slow to rapid growth is due to the temperature dependence of  $\langle \sigma v \rangle$  and  $f_i$ . As the ion temperature increases, the reaction rate, and hence the alpha heating source, increases as well. This drives both temperatures up, which leads to an increase in  $f_i$ , the fraction of the alpha energy which goes directly to the ions. However, the electron temperature is retarded by the radiation losses, and in both energy equations, the refueling term becomes larger as the reaction rate increases. Also the particle diffusion terms increase. These effects cause the temperatures to stop growing. At this point, the alpha particle density has not gone into steady state. The alpha density affects the electron energy balance through the radiation losses. The loss terms increase until the alpha density reaches steady state—this is the cause of the gradual decrease between the maximum temperatures and the steady state regime.

Qualitatively, the behavior of the non-local case is the same as the local case; see Figure 6(a,b,c)

and Table 6. The period of slow growth lasts longer in the non-local case. This is due to the same factor which causes the difference in the ignition requirements. Near the center of the plasma, the alpha heating source is not as intense in the non-local case as in the local case, because the center regions produce a larger fraction of the confined alpha energy than they absorb. Thus the temperatures will not increase as fast near the center, and the non-local case shows a longer period of slow growth. This same effect is also responsible for the lower growth rate of the non-local case once it reaches the rapid growth phase.

The growth rate for a quantity  $L$  is defined by:

$$\gamma_L = \frac{1}{L} \frac{\partial L}{\partial t} \quad (18)$$

The reciprocal of  $\gamma_L$  corresponds to the "e-folding" time. In both the local and non-local cases, the maximum electron temperature growth rate occurs at  $t = 0$ . This is because the initial ion and electron temperatures are the same. Thus  $W_{ei}$ , the collisional transfer term, does not retard the electron temperature initially. This initial jump in the electron temperature is of short duration and the associated growth rates for the two cases are within 2 per cent of each other. For the local case, the maximum growth rates are:  $\gamma_{W_n} = 0.393 \text{ sec}^{-1}$  at  $t = 5.38$  seconds, and  $\gamma_{T_i} = 0.160 \text{ sec}^{-1}$  at  $t = 5.80$  seconds. Evaluation of the non-local data gives  $\gamma_{W_n} = 0.330 \text{ sec}^{-1}$  at  $t = 7.21$  seconds and  $\gamma_{T_i} = 0.141 \text{ sec}^{-1}$  at  $t = 7.51$  seconds. As noted above, the time evolution of the non-local case is retarded with respect to the local case, here the time lag is about 1.7 seconds. Comparison of Tables 5 and 6 shows that the difference in the equilibrium values of the two cases is 4 percent or less. The major quantitative difference is between the growth rates;  $\gamma_{W_n}$  and  $\gamma_{T_i}$  are 16 and 12 percent smaller, respectively, in the non-local case.

The time behavior of some other cases was also studied. First, we will consider the lower density case; for these calculations the density on axis was  $2 \times 10^{20}$ . In the local case, the the growth rate is smaller than before because the reaction rate is lower, due to the low density. Because the growth rate is smaller for lower densities, the alpha particles build up gradually, and there is no overshoot of the equilibrium. Also, the instability will saturate at a lower level because the heat source is smaller. In the non-local case, the plasma is not ignited, but it does show a plateau-like behavior for a considerable period of time. The non-local case does not ignite because the greater temperatures needed to offset the non-local effect and the lower reaction rate increase the loss terms in the energy balance equations.

Next, we will consider the effects of using the energy deposition matrices given in Tables 3 and 4. The temperature and density on axis were 8.0 keV and  $3 \times 10^{20} \text{ m}^{-3}$  respectively. Figure 7(a,b,c)

gives the local case and Figure 8(a,b,c) is the non-local case. As in Figures 5 and 6, there is an initial period of slow growth, followed by rapid growth to a maximum, then a gradual decrease to equilibrium. However, the maximum growth rates are smaller than before. This is due to the smaller alpha heating source, which is a consequence of poorer alpha particle confinement. This is also the reason that the time of maximum growth occurs later in Figure 7 than in Figure 5. The equilibrium temperatures also reflect this; they are about 3 keV lower on axis.

The non-local case shows similar behavior. The larger non-local effects have increased the time lag between the local and non-local cases to about 15 seconds for this  $R_0 = 24$  case. Also the difference between the maximum growth rates in the local and non-local cases is approximately 25 per cent. In the  $R_0 = 48$  case, above, we found the difference to be about 15 percent.

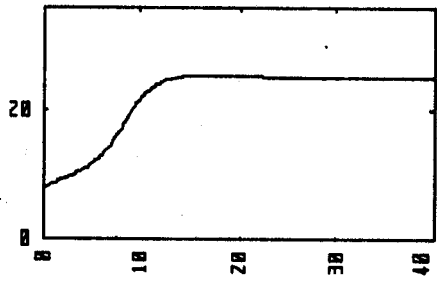
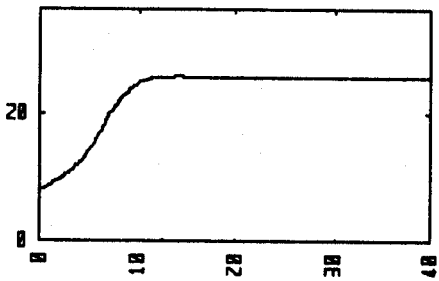
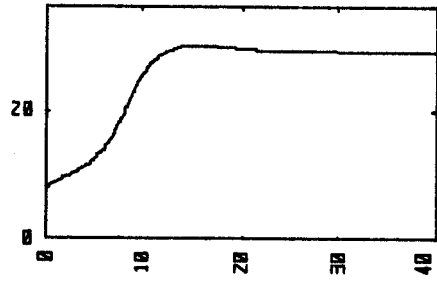
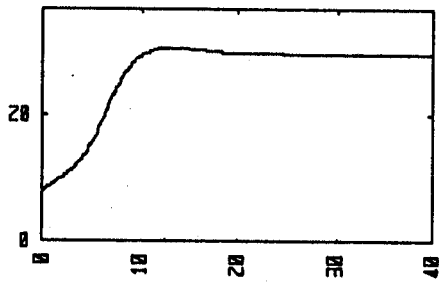
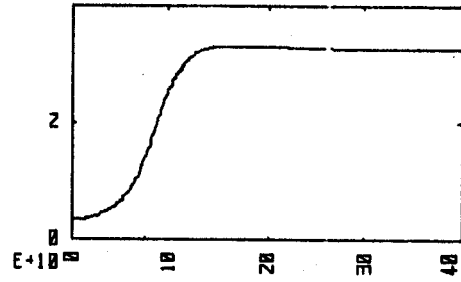
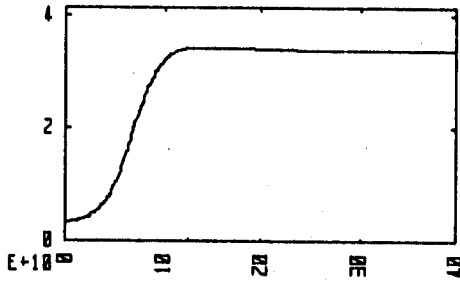


Figure 5: Local case  $T_o = 8.0$  keV

Figure 5(a):  $W_n$  vs. time

Figure 5(b):  $T_e$  vs. time

Figure 5(c):  $T_i$  vs. time

Figure 6: Non-Local case  $T_o = 8.0$  keV

Figure 6(a):  $W_n$  vs. time

Figure 6(b):  $T_e$  vs. time

Figure 6(c):  $T_i$  vs. time

Table 5: Local Equilibrium Conditions

TIME= 128.23019

|   | TI     | TE     | DNI        | DNE        | DNA        | RT    |
|---|--------|--------|------------|------------|------------|-------|
| 1 | 25.631 | 29.519 | 2.9876E+20 | 3.4953E+20 | 2.5386E+19 | 0.500 |
| 2 | 23.841 | 27.109 | 2.9481E+20 | 3.4431E+20 | 2.4750E+19 | 0.500 |
| 3 | 22.140 | 25.141 | 2.8895E+20 | 3.3708E+20 | 2.4063E+19 | 0.500 |
| 4 | 20.342 | 22.829 | 2.8216E+20 | 3.2884E+20 | 2.3342E+19 | 0.500 |
| 5 | 18.419 | 20.274 | 2.7407E+20 | 3.1918E+20 | 2.2555E+19 | 0.500 |
| 6 | 16.334 | 17.835 | 2.6394E+20 | 3.0738E+20 | 2.1722E+19 | 0.500 |
| 7 | 13.925 | 15.836 | 2.5110E+20 | 2.9261E+20 | 2.0755E+19 | 0.500 |
| 8 | 10.472 | 11.747 | 2.3631E+20 | 2.7545E+20 | 1.9567E+19 | 0.500 |
| 9 | 1.883  | 1.883  | 2.0089E+20 | 2.3409E+20 | 1.6603E+19 | 0.500 |

THERMAL OUTPUT 3.3746E+10 WATTS

Table 6: Non-Local Equilibrium Conditions

TIME= 133.97697

|   | TI     | TE     | DNI        | DNE        | DNA        | RT    |
|---|--------|--------|------------|------------|------------|-------|
| 1 | 25.195 | 29.253 | 2.9876E+20 | 3.4814E+20 | 2.4688E+19 | 0.500 |
| 2 | 23.307 | 26.452 | 2.9481E+20 | 3.4288E+20 | 2.4034E+19 | 0.500 |
| 3 | 21.580 | 24.146 | 2.8895E+20 | 3.3564E+20 | 2.3347E+19 | 0.500 |
| 4 | 19.837 | 22.041 | 2.8216E+20 | 3.2744E+20 | 2.2639E+19 | 0.500 |
| 5 | 17.994 | 19.871 | 2.7407E+20 | 3.1784E+20 | 2.1887E+19 | 0.500 |
| 6 | 15.968 | 17.395 | 2.6394E+20 | 3.0605E+20 | 2.1057E+19 | 0.500 |
| 7 | 13.638 | 15.464 | 2.5076E+20 | 2.9100E+20 | 2.0120E+19 | 0.500 |
| 8 | 10.292 | 11.681 | 2.3561E+20 | 2.7351E+20 | 1.8948E+19 | 0.500 |
| 9 | 1.883  | 1.883  | 1.9959E+20 | 2.3167E+20 | 1.6042E+19 | 0.500 |

THERMAL OUTPUT 3.2605E+10 WATTS

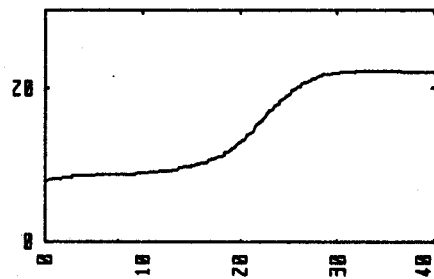
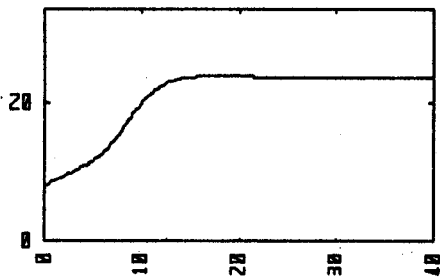
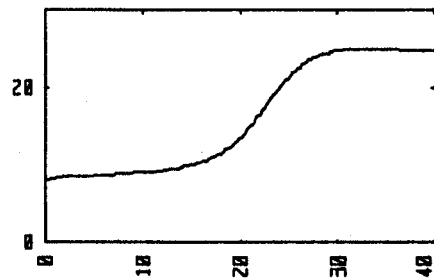
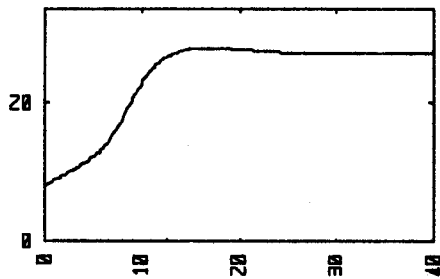
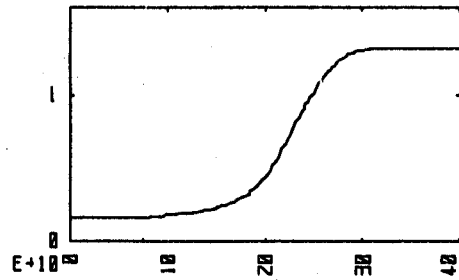
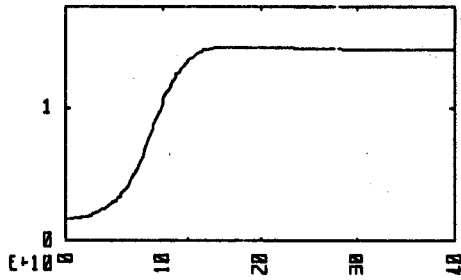


Figure 7: Local case  $R_0 = 24$  m  $T_0 = 8$  keV

Figure 8: Non-Local case  $R_0 = 24$  m  $T_0 = 8$  keV

Figure 7(a):  $W_n$  vs. time

Figure 8(a):  $W_n$  vs. time

Figure 7(b):  $T_e$  vs. time

Figure 8(b):  $T_e$  vs. time

Figure 7(c):  $T_i$  vs. time

Figure 8(c):  $T_i$  vs. time

## Section 6. Stability of the Steady State Regimes

In this section, the stability of the equilibria found in the previous section, against a step perturbation in the electron temperature, is studied. The method employed is to use the equilibrium values (see Tables 5 and 6) for the input data, with the values of  $T_e$  increased by 10 per cent everywhere except at the separatrix. The code TORSE is used to follow the time behavior of the electron and ion temperatures, and the integrated neutron power.

With this step perturbation in  $T_e$ ,  $W_{ei}$  will increase and  $f_c$  will decrease. The result of these two factors is first an increase in  $T_i$ , which will raise  $W_n$ , and a decrease in  $T_e$ . Thus, if the system is stable, the perturbation in  $T_e$  should be damped and the system should return smoothly to the equilibrium<sup>[11,12]</sup>. This is indeed the result. For both the local and non-local energy deposition cases the temperature and density values return to within 0.5 per cent of the equilibrium values. Comparison of the two cases shows that the perturbation is almost completely damped out after 4 seconds. The damping rate is slightly larger in the local case. The rise times of  $W_n$  and  $T_i$  do not differ significantly in the two cases. There is a slight undershoot of the equilibrium, but it is very small for both cases. Thus there is little difference between the two cases in their stability against electron temperature perturbations.

## Section 7. Summary and Conclusions

Thus far, a comparison of the non-local and local energy deposition cases has been made in the areas of ignition requirements, growth rates of the thermal instability and equilibrium values of temperature and density, and stability of the equilibria against a perturbation in the electron temperatures. The higher temperatures needed for ignition in the non-local case are expected because of the greater loss of alpha energy from the central regions, compared to the local case. The difference in the growth rates of the thermal instability can be explained by the same mechanism.

There appears to be little difference in the equilibrium states or in the response to the perturbation in the electron temperature.

We have found that the plasma achieves stability when the peak ion temperature is between 25 and 26 keV. In reference 12, a similar analysis of the energy balance equations is carried out for different diffusion models; the Bohm diffusion coefficient, a constant coefficient, and the classical diffusion coefficient. The critical temperature is defined as the centerline ion temperature above which the plasma is stable. The classical case gives a critical temperature of 38 keV, the Bohm scaling gives 14 keV, and the constant diffusion coefficient yields a critical temperature of 24 keV. A value of 28 keV is found



for the constant coefficient case in reference 13. Our value of approximately 25 keV is much less than the classical 38 keV, which is to be expected, because of the use of neoclassical plateau scaling in the diffusion coefficient. The value of 25 keV is larger than the Bohm diffusion derived 14 keV, but this also to be expected from the diffusion scaling that we employed. In reference 14, the critical temperature is examined as a function of the poloidal  $\beta$ . The values of the critical temperature lie between 20 and 30 keV. In reference 15, thermal stability is achieved for  $T_i \approx 50$  keV. Here the cyclotron radiation loss and the build up of alpha particles have been neglected, so the critical temperature would be expected to be higher than those found in this paper. Thus the critical temperatures for both the local and non-local cases are in general agreement with the literature.

We have also considered lower densities plasma densities and other energy deposition matrices. At lower densities, the non-local effects were found to increase in importance. The other set of energy deposition matrices model the effects of poorer alpha confinement and an increase in the non-local nature of the energy deposition. The poorer confinement of the alpha energy results in a higher temperature needed for the plasma to be ignited. Also, the difference in ignition temperatures for the local and non-local cases is larger. This is because of the relatively larger off-diagonal elements in the energy deposition matrix. The increase of the non-local effects is also seen in the larger difference between the local and non-local growth rates. This is an important consideration, because in an actual toratron reactor, there may be factors, such as bumpy fields due to the modularity of the coil design, which could increase the non-local nature of the energy deposition.

In conclusion, it seems that non-local alpha energy deposition has both disadvantages and advantages. The non-local effect will require the plasma to be heated externally to a higher initial temperature than would be needed if the energy deposition was local. Once the plasma is ignited, and auxiliary heating is no longer needed, the non-local effect is favorable. The thermal instability takes a few seconds longer to exhibit rapid growth than the local case, and the maximum growth rates are lower than local case. This is a positive factor from the standpoint of fusion reactor control.

## References

1. R. E. Potok, *Particle Orbits and Diffusion in Torsatrons*, Sc.D.thesis, Dept. of Nuclear Engineering, Massachusetts Institute of Technology, (May, 1980).
2. S. I. Braginskii, "Transport Processes in a Plasma," *Reviews of Plasma Physics*, Vol. 1, Consultants Bureau, New York, (1965).
3. J. W. Johnson, *The Effect of Non-Local Alpha Energy Deposition on Torsatron Reactors*, S.M.thesis, Dept. of Nuclear Engineering, Massachusetts Institute of Technology, (May, 1981).
4. F. L. Hinton, R. D. Hazeltine, *Rev. Mod. Phys.* **48**, 239, (1976).
5. R. N. Byrne, *et al*, *Tokamak Reactor Codes: MAKO and MAKI (EPRI Report ER-1032)*, Electric Power Research Institute, (March, 1979).
6. A. A. Galeev, R. Z. Sagdeev, *Sov. Phys.-JETP* **26**, 233, (1968).
7. J. Greene, *Astrophys. J.* **130**, 693, (1959).
8. L. Spitzer Jr., *Physics of Fully Ionized Gases*, John Wiley and Sons, New York, (1962).
9. M. N. Rosenbluth, *Nucl. Fusion* **10**, 340, (1970).
10. D. J. Rose, *Nucl. Fusion* **9**, 183, (1969).
11. H. Saito, T. Sekiguchi, M. Katsurai, S. Maekawa, *Nucl. Fusion* **17**, 919, (1977).
12. H. D. Campbell, J. L. Usher, *Trans. Amer. Nucl. Soc.* **21**, 45, (1975).
13. M. Ohta, H. Yamato, S. Mori, *J. Nucl. Sci. Technol.* **10**, 353, (1973).
14. W. M. Stacey, *Nucl. Fusion* **15**, 63, (1975).
15. L. Bromberg, D. R. Cohn, J. L. Fisher, *Nucl. Fusion* **19**, 1359, (1975).